Earthquake Engineering & Structural Dynamics
The Journal of the International Association for Earthquake Engineering

EARTHQUAKE ENGINEERING & STRUCTURAL DYNAMICS
*Earthquake Engng Struct. Dyn.* 2014; **43**:889–908
Published online 16 October 2013 in Wiley Online Library (wileyonlinelibrary.com). DOI: 10.1002/eqe.2378

# Evaluation of a recently proposed record selection and scaling procedure for low-rise to mid-rise reinforced concrete buildings and its use for probabilistic risk assessment studies

Bekir Özer Ay and Sinan Akkar*,†

*Earthquake Engineering Research Center, Department of Civil Engineering, Middle East Technical University, 06800 Ankara, Turkey*

SUMMARY

This paper evaluates a recent record selection and scaling procedure of the authors that can determine the probabilistic structural response of buildings behaving either in the elastic or post-elastic range. This feature marks a significant strength on the procedure as the probabilistic structural response distribution conveys important information on probability-based damage assessment. The paper presents case studies that show the utilization of the proposed record selection and scaling procedure as a tool for the estimation of damage states and derivation of site-specific and region-specific fragility functions. The method can be used to describe exceedance probabilities of damage limits under a certain target hazard level with known annual exceedance rate (via probabilistic seismic hazard assessment). Thus, the resulting fragility models can relate the seismicity of the region (or a site) with the resulting building performance in a more accurate manner. Under this context, this simple and computationally efficient record selection and scaling procedure can be benefitted significantly by probability-based risk assessment methods that have started to be considered as indispensable for developing robust earthquake loss models.


Received 4 April 2013; Revised 13 August 2013; Accepted 16 September 2013

KEY WORDS: record selection and scaling; linear and nonlinear structural response; probability-based risk assessment; probability-based damage assessment; fragility functions

## 1. INTRODUCTION

Estimating seismic induced risk is a challenging subject as it has to consider structural and ground-motion uncertainties at the same time. The rationale behind this fact stems from the random nature of earthquakes and complexity of structural behavior against seismic action. The interaction between these two components results in complications at the modeling and analysis level of the problem that eventually jeopardizes the reliability of seismic risk assessment studies. The necessity of considering the interaction between complex earthquake phenomena and structural response becomes even more evident for risk assessment methods that employ response history analysis (RHA) for estimating the likely damage state of structures for a predetermined hazard level (e.g., [1, 2]). These methods require a set of accelerograms of similar strong-motion characteristics to simulate the target seismic activity and to ensure a reasonable accuracy in structural response estimations. The properly selected accelerograms would realistically describe the record-to-record variability that in turn results in coherent structural response estimations. The major difficulty of this approach is the collection of records fulfilling the

*Correspondence to: Sinan Akkar, Earthquake Engineering Research Center, Department of Civil Engineering, Middle East Technical University, 06800 Ankara, Turkey.
†E-mail: sakkar@metu.edu.tr

strict requirements of target hazard scenario. The strong-motion databases are still far from providing sufficiently enough accelerograms to comply with the entire constraints imposed by the specific case in hand. Alternatively, scaling of properly selected ground-motion records can be used to warrant the accelerograms having similar strong-motion characteristics with the aim of accurate estimation of structural response. This way, the analyst can obtain reliable information on the seismic performance of structural systems for a given target seismic intensity without suffering from the insufficiency of ground-motion data.

The current record selection and scaling methods are conditioned either on a target intensity level (e.g., [3]) or on a target response spectrum (e.g., [4, 5]). The primary aim in most of these procedures is to scale a sufficient number of accelerograms for nonlinear RHA to ensure an accurate estimation of median structural response with minimum dispersion. Recent studies emphasize the consideration of scatter about target hazard level together with median structural response to represent a more realistic structural behavior because of inherent uncertainty in ground motions as well as their interaction with structures [6–8]. To this end, several studies proposed record selection and scaling methodologies that account for a reasonable dispersion about target hazard level (e.g., [6, 9–11]). As part of these studies, Jayaram *et al*. [6] suggested the use of zero variance scaling when target hazard inherently accounts for a certain level of variability over median seismic demand (e.g., uniform hazard spectrum (UHS) or design spectrum).

This paper evaluates a recently proposed ground-motion record selection and scaling procedure [12] that can be considered among the procedures summarized in the previous paragraph. The procedure accounts for the scatter about target hazard level. It estimates the standard deviation of scaled accelerograms about target hazard to identify the optimum recording set from a suite of candidate accelerograms. The optimum recording set yields the least dispersion about target hazard level, and the median spectral ordinate of scaled accelerograms exactly matches with the target elastic spectral ordinate. The procedure is equally applicable for linear and nonlinear structural behavior. The major aim of evaluating Ay and Akkar [12] is to verify its usability in probability-based risk assessment studies. The first part of the paper focuses on the verification of this procedure for estimating the damage distribution of low-rise to mid-rise reinforced concrete (RC) moment resisting frame (MRF) systems. The rest of the paper presents the implementation of the procedure for deriving site-specific or region-specific building fragility functions that constitute one of the primary components in probabilistic seismic risk assessment. This is achieved by discussing the results of case studies that are tailored by considering the limitations of the proposed record selection and scaling procedure.

## 2. OVERVIEW OF THE GROUND-MOTION RECORD SELECTION AND SCALING METHODOLOGY

Detailed explanations about the proposed procedure are given in Ay and Akkar [12]. This section briefs the essentials of the method for the reader to follow the discussions on its implementation while determining building damage states and probabilistic seismic risk assessment studies. The explanations about the procedure are performed by using spectral displacement ($S_d$) as the recent damage assessment studies use this parameter intensively (e.g., [13]). However, it is equally applicable to all ground-motion intensity measures including spectral acceleration, peak ground acceleration, and velocity [14].

The Ay and Akkar [12] procedure linearly scales ground-motion recordings to a target elastic spectral ordinate ($\overline{S}_{dt\,\mathrm{arget}}(T)$) by preserving the inherent uncertainty (aleatory variability) in the selected accelerograms. The elastic target spectral ordinate can be obtained from the deaggragation of a site-specific probabilistic seismic hazard assessment (PSHA). Using a set of record selection criteria [12], the method selects and scales $n$ records from $k$ candidate accelerograms that yield the least dispersion about the target elastic spectral ordinate. Thus, the proposed methodology scales a total of $C(k,n)$ sets of ground motions and selects the optimum set among them with the minimum dispersion about target elastic spectral ordinate. Here, $C(k,n)$ refers to the combination number of ground-motion bins of $n$ records selected from $k$ candidate accelerograms. In essence, the method has a nested record selection



DOI: 10.1002/eqe

and scaling structure and has the advantage of computing the dispersion of scaled accelerograms about target spectral ordinate. The aforementioned advantage will be used to describe the distribution of global structural response in the subsequent sections.

The procedure constrains the scaling to a parameter ($\varepsilon\sigma_{Sdi}$) defined as the logarithmic difference between the elastic spectral displacement of the *ith* record, $S_{d,i}(T)$, and the corresponding median ground motion ($\overline{S}_{d,i}(T)$) estimated from a representative ground-motion prediction equation (GMPE). Equation (1) describes the calculation of $\varepsilon\sigma_{Sdi}$.

$$\varepsilon\sigma_{\mathrm{Sdi}} = \ln\left(S_{d,i}\right) - \ln\left(\overline{S}_{d,i}\right) \tag{1}$$

The use of $\varepsilon\sigma_{Sdi}$ enables the scaling procedure to linearly modify each accelerogram to its individual target level instead of scaling all records to the target spectral ordinate (e.g., [3]). The individual target levels are computed by using a parameter called as scaling origin, $\theta$. The average of individual target levels of scaled accelerograms matches with the target spectral displacement, $\overline{S}_{dt\,\mathrm{arget}}(T)$. Equation (2) shows the calculation of $\theta$.

$$\theta = \ln\left(\overline{\mathrm{S}}_{\mathrm{dt\,arget}}\right) - \ln\left(\frac{\sum_{i=1}^{n}\exp(\varepsilon\sigma_{\mathrm{Sdi}})}{n}\right) \tag{2}$$

As stated in the previous paragraph, the parameter $n$ in Equation (2) is the total number of records in the scaled ground-motion bin. The procedure modifies each individual record, $i$, with its scaling factor, $\gamma_i$. The computation of $\gamma_i$ is given in Equation (3).

$$\gamma_i = \frac{S_{dt\,\mathrm{arget},i}(T)}{\mathrm{S_{d,i}}(T)} = \frac{\exp(\theta + \varepsilon\sigma_{Sdi})}{\mathrm{S_{d,i}}(T)} \tag{3}$$

As one can infer from Equation (3), $S_{dtarget,i}$ is a linear function of $\varepsilon\sigma_{Sdi}$ for elastic systems. The linear relationship established between individual target levels and $\varepsilon\sigma_{Sdi}$ fails for structures responding beyond their elastic capacities [12]. Thus, Ay and Akkar [12] proposed an alternative parameter, $\varepsilon\sigma_{ISdi}$ that correlates better with inelastic structural response to obtain the optimum ground-motion bin with minimum dispersion about median nonlinear structural response. This alternative parameter is based on the nonlinear response of equivalent SDOF systems that represent the actual building behavior of first-mode dominant structures. It is a linear combination of ($\varepsilon\sigma_{Sdi}$) and ($\varepsilon\sigma_{PGV}$). The latter parameter is the logarithmic difference between the peak ground velocity (PGV) of the *ith* record, and the corresponding median ground motion estimated from a GMPE (if possible, the authors urge to use a ground-motion predictive model that can estimate both spectral ordinates as well as PGV for internal consistency in the calculations). The expressions for the computation of $\varepsilon\sigma_{ISdi}$ are given in Equation (4). The inelasticity level of the equivalent SDOF system is described by the strength reduction factor, $R$ (ratio of elastic-to-yield pseudo-spectral acceleration or, alternatively, ratio of elastic-to-yield spectral displacement). When the structure behaves in the elastic range (i.e., $R = 1$), $\varepsilon\sigma_{ISdi}$ automatically becomes $\varepsilon\sigma_{Sdi}$.

$$\varepsilon\sigma_{\mathrm{ISdi}} = c_1(R,T)\cdot\varepsilon\sigma_{\mathrm{Sdi}} + c_2(R,T)\cdot\varepsilon\sigma_{\mathrm{PGV}} + c_3(R,T) \tag{4a}$$

$$c_1(\mathrm{R},\mathrm{T}) = 1 - 0.72\ln(\mathrm{R}) + 0.7T\ln(\mathrm{R}) - 0.21T^2\ln(\mathrm{R}) \tag{4b}$$

$$c_2(\mathrm{R},\mathrm{T}) = 0.81\ln(\mathrm{R}) - 0.78T\ln(\mathrm{R}) + 0.23T^2\ln(\mathrm{R}) \tag{4c}$$

$$c_3(\mathrm{R},\mathrm{T}) = 0.22\ln(\mathrm{R}) - 0.4T\ln(\mathrm{R}) + 0.15T^2\ln(\mathrm{R}) \tag{4d}$$



DOI: 10.1002/eqe

Assuming that the distribution of inelastic spectral response of scaled recordings is log-normal, its expected value ($\lambda_{Sdtarget}$) and standard deviation ($\zeta_{Sdtarget}$) can be estimated by using Equations (5) and (6), respectively. The parameter $\mu_{\varepsilon\sigma}$ is the average of $\varepsilon\sigma_{ISdi}$ values computed from $n$ recordings. These equations express the log-normal distribution of inelastic spectral response of interest after the implementation of scaled ground motions for a target spectral ordinate. However, they can also give a reasonable proxy of nonlinear building response for estimating likely damage states as well as probability-based risk assessment. These particular features of the proposed procedure are discussed in the following sections.

$$\lambda_{S_{dtarget}} = \theta + \frac{\sum_{i=1}^{n} \varepsilon\sigma_{ISdi}}{n} = \theta + \mu_{\varepsilon\sigma} \tag{5}$$

$$\zeta_{S_{dtarget}} = \sqrt{\frac{1}{n-1} \cdot \sum_{i=1}^{n} \left(\varepsilon\sigma_{ISdi} - \mu_{\varepsilon\sigma}\right)^2} \tag{6}$$

Note that the modified method for nonlinear structural response selects and scales the records in the optimum ground-motion bin such that the average elastic spectral ordinates of the modified records exactly match with the target elastic spectral level. This is another advantage of the proposed method as conventional seismic hazard assessment still yields elastic spectral ordinates for target hazard scenario as ground-motion prediction equations estimating the nonlinear ground-motion intensity parameters are currently very few (e.g., [15–18]). These predictive models focus on different nonlinear ground-motion demands and being very few in number may result in insufficient modeling of epistemic uncertainty in PSHA when different seismotectonic regimes are of concern [19]. Although some of the record selection and scaling procedures for nonlinear structural response modify elastic spectral demands by some factors to account for nonlinear ground-motion demands, the resulting nonlinear spectral quantity may not confirm the nonlinear target hazard at the predefined return period as these modifying factors cannot be properly incorporated with the hazard integral. Further discussions on such record selection and scaling methods are given in the following sections.

## 3. EVALUATION OF THE PROPOSED METHODOLOGY FOR BUILDING (MDOF) SYSTEMS

The procedure by Ay and Akkar [12] is evaluated by comparing its performance with two alternative record selection and scaling procedures proposed by Baker [5] and Kalkan and Chopra [20]. Subsequent sections present the analytical building models and the target hazard scenario used for the comparisons of structural response statistics obtained from these record selection and scaling procedures. The methods by Baker [5] and Kalkan and Chopra [20] are briefly described in the following subsections as well. The reader is referred to the cited references for an in-depth understanding about each method.

### *3.1. Structural models and analyses*

Three MRF models (3-story, 4-story, and 8-story) are designed that comply with the Turkish Earthquake Code (TEC) [21], as well as TS 500-2000 [22] and TS 498 [23]. The latter two codes define the material properties and contain provisions for RC building design against vertical loads. PROBINA ORION (Prota Software Inc., Ankara, Turkey) [24] software is used in the design of buildings. The characteristic concrete strength is taken as 20 MPa, and the yield strength of steel is 420 MPa. The buildings are assumed to be located in the proximity of active faults (seismic zone 1 according to TEC [21]). The site condition is chosen as soft soil (classified as Z3 in TEC [21]) that



DOI: 10.1002/eqe

can be approximately characterized with a $V_{S30}$ variation between 180 and 360 m/s. These descriptions indicate that the evaluations and investigations presented in this paper are limited to the analyses of code-complying buildings that have invariant material properties.

Figure 1 describes the geometries of 3-story, 4-story, and 8-story frames used in the comparison of three record selection and scaling methods. The story heights and span lengths of each model are given on this figure as well. Figure 1 also shows the cross-sectional dimensions of column and beam members of the models. The column cross-sectional area is reduced toward upper stories: a common application in the Turkish construction practice.

The nonlinear static pushover analysis and RHA of frame models are performed by using the SEISMOSTRUCT (Seismosoft, Pavia, Italy) [25] platform (version 5.2.2). The software employs Hilber–Hughes–Taylor integration method [26] while performing nonlinear RHA. The frame members are modeled as inelastic force-based fiber elements [27]. Nonlinear concrete model of Mander *et al*. [28] and bilinear steel model are used to represent material nonlinearity.

Modal parameters of the frames are determined by eigenvalue analysis. Nonlinear static pushover analyses are performed to obtain the capacity curves (pushover curves) of each frame. An invariant lateral load pattern corresponding to the first-mode shape is used in the pushover analysis [29]. Roof displacement versus base shear relationship of each building is idealized as a bilinear force-deformation curve according to the ATC-40 [30] procedure. The corresponding acceleration versus displacement response spectra (ADRS, [31]) of each frame is obtained by using the idealized bilinear capacity curves and modal parameters. This way, the MDOF models are approximated as equivalent SDOF systems defined with fundamental period, $T_1$, yield spectral displacement, $S_{d,y}$ (elastic displacement capacity), yield spectral acceleration, $PS_{a,y}$ (elastic strength capacity), and post-yield stiffness ratio, $\alpha$. Table I lists the fundamental dynamic features of each frame model.

The eigenvalue analysis of 3-story and 4-story frames yield the first-mode periods as 0.50 and 0.61 s, respectively. The translational effective modal mass participation of the fundamental mode is found as 0.87 for the 3-story frame, whereas it is 0.84 for the 4-story frame. The fundamental mode period and corresponding modal mass participation of 8-story frame is 1.12 s and 0.78, respectively. Note that 3-story and 4-story structures show a first-mode dominant behavior, whereas the eigenvalue analysis of 8-story frame suggests a first-mode behavior with a certain level of higher mode contribution.

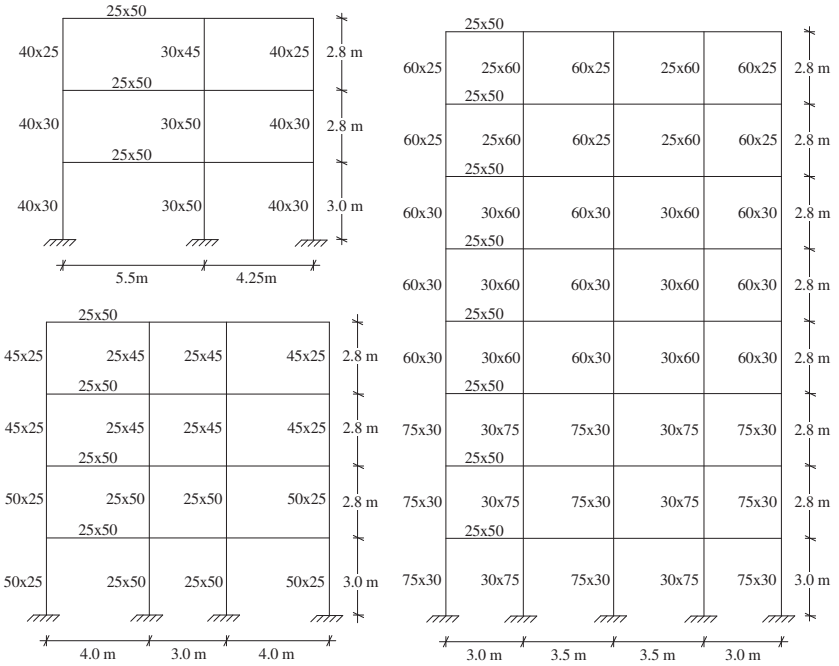


Figure 1. 3-story, 4-story, and 8-story frame models and corresponding member dimensions.



DOI: 10.1002/eqe

Table I. Idealized equivalent SDOF system properties of frame models.

| Fundamental dynamic parameters | 3-story | 4-story | 8-story |
|---|---|---|---|
| $T_1$ (s) | 0.50 | 0.61 | 1.12 |
| Γ* | 0.87 | 0.84 | 0.78 |
| α (%) | 2.10 | 3.03 | 0.70 |
| $S_{d,y}$ (cm) | 2.85 | 3.35 | 6.48 |
| $PS_{a,y}$ (g) | 0.45 | 0.36 | 0.21 |
| η† | 0.39 | 0.30 | 0.16 |

*Γ: Modal mass participation of fundamental mode
†η: Base shear coefficient (yield base shear normalized by building weight).

The inelastic spectral analyses of idealized SDOF systems and nonlinear RHA of MDOF systems are performed by using the records selected and scaled by each record selection and scaling methodology. Maximum roof drift ratio (MRDR; maximum roof displacement normalized with building height) is used as the global building response parameter. The median building responses and corresponding dispersion statistics are discussed in Section 3.3 to verify the performance of three alternative selection and scaling methods.

### *3.2. Probabilistic seismic hazard assessment study and target earthquake scenario*

A target earthquake scenario is used for the comparisons of alternative procedures. Assuming that the sample buildings are located near the city of Erzurum in Eastern Anatolia; the expected seismic hazard is computed by site-specific PSHA. The strike-slip North Anatolian and East Anatolian faults as well as the Erzurum Fault are considered as the seismic sources that are likely to produce the future earthquakes in the area of interest. The Akkar and Bommer [32] GMPE is used for ground-motion modeling in PSHA. The UHS of 2475-years return period ($T_R = 2475$ years) is assumed to represent the ground motions generated by the maximum considered earthquake of the considered region.

The most contributing earthquake scenario to the 2475-years UHS (i.e., $M_w$-$R_{JB}$ pair) is determined from the deaggregation analysis. The Erzurum fault of 80 km in length that is located approximately 3 km from the southern part of the site is identified as the most contributing seismic source. The deaggregation results for each building model for $T_R = 2475$ years are given in Figure 2. The moment magnitude ($M_w$) and source-to-site distance ($R_{JB}$; Joyner and Boore [33]) of the most contributing earthquake scenario for each model building are summarized in Table II. As one can infer from Figure 2 and Table II, the magnitude and distance information of the most contributing earthquake scenario is the same for all building models. The most contributing earthquake represents the target earthquake scenario for the record selection and scaling methods evaluated here. The corresponding target spectral ordinates ($\overline{S}_{dt\,arget}$) that are obtained from the Akkar and Bommer [32] predictive model are also given in Table II.

### *3.3. Comparisons of selection and scaling procedures*

*3.3.1. Final selection and scaling of ground-motion records.* A total of 20 candidate accelerograms are assembled according to the magnitude, distance, and site class information of the target earthquake scenario presented in the previous section. The ground motions are compiled from the PEER-NGA strong-motion database (http://peer.berkeley.edu/peer_ground_motion_database) as well as the Turkish strong-motion database (http://kyh.deprem.gov.tr/ftpe.htm). As all buildings are located on site class Z3 [21], the soil conditions of selected candidate accelerograms depict either site class Z2 or site class Z3 features. Site class definitions of Z2 and Z3 can be considered as the counterparts of site classes C and D in NEHRP/P-750 document [34]. Detailed information about the criteria employed in the identification of candidate ground-motion dataset can be found in Ay [14]. The overall characteristics of candidate accelerograms are listed in Table III.

Each tested methodology selects and scales an optimum ground-motion bin of 10 accelerograms from the candidate ground-motion recordings. The proposed methodology identifies the optimum



DOI: 10.1002/eqe

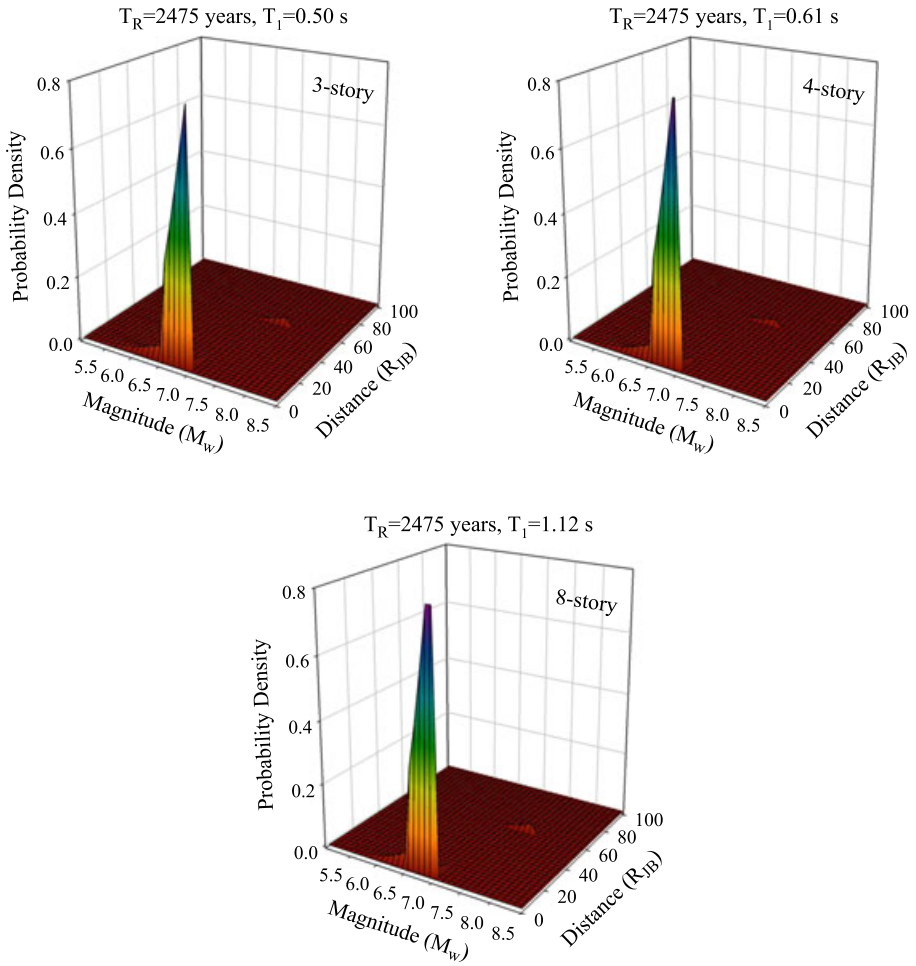


Figure 2. Probabilistic seismic hazard assessment deaggregation results of the case study for $T_R = 2475$ years. First raw, left and right panels show the deaggregation results for $T_1 = 0.50$ s (3-story model), and $T_1 = 0.61$ s (4-story model), respectively. Deaggregation result of the 8-story building ($T_1 = 1.12$ s) is shown on the second row.

Table II. The most contributing earthquake scenario and corresponding spectral displacements for each building model.

| | 3-story | 4-story | 8-story |
|---|---|---|---|
| $M_{w,target}$ | 6.95 | 6.95 | 6.95 |
| $R_{JB,target}$ (km) | 3.75 | 3.75 | 3.75 |
| $\overline{S}_{dt\,target}$ ($T_1$) (cm) | 12.38 | 17.01 | 34.33 |

ground-motion bin through the estimations of dispersion about nonlinear spectral response. It ranks the estimated dispersion (Equation (6)) of each alternative ground-motion bin of 10 records assembled from the candidate ground-motion dataset. A total of 184,756 ground-motion bins, each having a different set of ground-motion records, are assembled during this step. The entire computational time of this step is 3 min on a regular PC with a common i7 processor and 4.00 GB RAM. As indicated in Section 2, the average elastic spectral ordinates of the scaled records in the optimum ground-motion bin exactly matches with the elastic target spectral level.

The record selection and scaling method proposed by Baker [5] use amplitude scaling of ground motions according to the elastic spectral ordinates. Baker [5] constrains the selection of recordings to match conditional mean spectrum (CMS) (a target spectral shape conditioned on the occurrence



DOI: 10.1002/eqe

Table III. Major seismological parameters of the candidate recording set.

| Record name | Earthquake name | Recording station | $M_w$ | $R_{JB}$ (km) | $V_{S30}$ (m/s) | Fault type* |
|---|---|---|---|---|---|---|
| PEER0289 | Irpinia, Italy, 1980 | Calitri | 6.9 | 13.3 | 600 | N |
| PEER0290 | Irpinia, Italy, 1980 | Mercato San Severino | 6.9 | 29.8 | 350 | N |
| PEER0764 | Loma Prieta, CA, 1989 | Gilroy - Historic Bldg. | 6.9 | 10.3 | 339 | SS |
| PEER0801 | Loma Prieta, CA, 1989 | San Jose - Santa Teresa Hills | 6.9 | 14.2 | 672 | SS |
| PEER0809 | Loma Prieta, CA, 1989 | UCSC | 6.9 | 12.2 | 714 | SS |
| PEER0968 | Northridge, CA, 1994 | Downey - Co Maint Bldg | 6.7 | 43.2 | 272 | RV |
| PEER0971 | Northridge, CA, 1994 | Elizabeth Lake | 6.7 | 36.2 | 235 | RV |
| PEER1005 | Northridge, CA, 1994 | LA - Temple & Hope | 6.7 | 28.8 | 376 | RV |
| PEER1042 | Northridge, CA, 1994 | N Hollywood - Coldwater Can | 6.7 | 7.9 | 446 | RV |
| PEER1052 | Northridge, CA, 1994 | Pacoima Kagel Canyon | 6.7 | 5.3 | 508 | RV |
| PEER1078 | Northridge, CA, 1994 | Santa Susana Ground | 6.7 | 1.7 | 715 | RV |
| PEER1116 | Kobe, Japan, 1995 | Shin - Osaka | 6.9 | 19.1 | 256 | SS |
| PEER1144 | Gulf of Aqaba, Egypt, 1995 | Eilat | 7.2 | 43.3 | 355 | SS |
| PEER1776 | Hector Mine, CA, 2003 | Desert Hot Springs | 7.1 | 40.4 | 685 | SS |
| PEER1794 | Hector Mine, CA, 2003 | Joshua Tree | 7.1 | 31.1 | 379 | SS |
| PEER1795 | Hector Mine, CA, 2003 | Joshua Tree N.M. - Keys View | 7.1 | 50 | 685 | SS |
| TGMB1584 | Duzce, Turkey, 1999 | Sakarya Karadere - 9907 | 7.1 | 3.7 | 316 | SS |
| TGMB1585 | Duzce, Turkey, 1999 | Sakarya Karadere - 9904 | 7.1 | 0 | 440 | SS |
| TGMB1591 | Duzce, Turkey, 1999 | Sakarya Karadere - 9906 | 7.1 | 6.1 | 456 | SS |
| TGMB1594 | Duzce, Turkey, 1999 | Sakarya Karadere - 9901 | 7.1 | 0 | 481 | SS |

*N is normal faulting, RV is reverse faulting, and SS is strike-slip faulting.



DOI: 10.1002/eqe

of a target intensity level associated with deaggregation results). The record selection is performed for a predetermined period interval (suggested as $0.2\,T_1$ and $2.0\,T_1$ by Baker [5]) to consider the structural period variation due to inelastic response and higher mode effects. The correlation coefficients that account for the variation of spectral ordinates with respect to the target spectral ordinate at the fundamental building period are taken from Baker and Cornell [35] while computing CMS.

The third method [20] considers a close match between inelastic spectral ordinate of target scenario and selected ground motions. Consequently, this method computes the strength reduction factor, $R$, to modify the elastic target spectral ordinate for the corresponding inelastic spectral ordinate (i.e., target inelastic spectral ordinate; $\overline{S}_{dit\,\mathrm{arg}et}$). Given a building model $R$ is calculated by normalizing the elastic target spectral ordinate with the yield spectral ordinate of the building that is computed from its idealized capacity spectrum (i.e., $R=\overline{S}_{dt\,\mathrm{arg}et}/S_{d,y}$). The computed $R$ value is used in an empirical relationship (generally referred to as $C_R$ in the literature; [36]) to compute the expected inelastic spectral displacement from the corresponding elastic spectrum. For the case study presented in this paper, the yield spectral displacement ($S_{d,y}$) and target elastic spectral displacement ($\overline{S}_{dt\,\mathrm{arg}et}(T_1)$) values for each frame are given in Tables I and II, respectively. Note that the strength reduction factor is $R=4.4$ for a 3-story frame, whereas $R=5.1$ and $R=5.3$ for 4-story and 8-story frames, respectively. The Kalkan and Chopra [20] method scales each candidate ground motion iteratively until the target inelastic spectral displacement is achieved. This iterative step can take a significant amount of time as the nonlinear SDOF response and scaling factor to obtain $\overline{S}_{dit\,\mathrm{arg}et}(T_1)$ are not linearly correlated.

Table IV lists the candidate ground-motion dataset and the recordings selected by each methodology from this dataset. The columns labeled as AA12 show the records selected and scaled by the Ay and Akkar [12] procedure, whereas abbreviations B11 and KC11 display the records selected and scaled by Baker [5] and Kalkan and Chopra [20], respectively. The scaling factors used for modifying the selected accelerograms are also listed in Table IV. Note that scaling factors of selected records that are common in these methods attain similar values. Some of the scaling factors are very high. As the candidate accelerogram dataset is the same for all compared procedures, the performance evaluations of these methods are performed in an objective manner by the considered case studies. We note that the CMS exercise is also repeated by using the correlation coefficients proposed by

Table IV. Optimum ground-motion records identified by the compared procedures and corresponding scaling factors.

| | 3-story | | | 4-story | | | 8-story | | |
|---|---|---|---|---|---|---|---|---|---|
| Record Name | AA12 | B11 | KC11 | AA12 | B11 | KC11 | AA12 | B11 | KC11 |
| PEER0289 | 5.72 | 5.32 | 4.81 | 5.63 | | 5.21 | 5.72 | 4.05 | 4.96 |
| PEER0290 | 8.49 | | 8.38 | 8.32 | 7.96 | | 7.19 | | |
| PEER0764 | 3.24 | 3.28 | 4.34 | 3.17 | 4.80 | 3.47 | 2.92 | 3.00 | 3.40 |
| PEER0801 | 5.43 | 4.53 | | 5.42 | 3.64 | | 5.67 | | |
| PEER0809 | | | | | | | | | |
| PEER0968 | | | | | | 6.49 | 11.03 | | |
| PEER0971 | 8.68 | 7.78 | 9.21 | 9.17 | | | 9.44 | | |
| PEER1005 | | 5.83 | | | 6.04 | 7.79 | | 7.61 | 7.40 |
| PEER1042 | 3.34 | | | 3.48 | 4.07 | 4.08 | 4.27 | 3.38 | 3.52 |
| PEER1052 | 2.79 | 2.07 | 2.27 | 2.82 | 2.02 | 2.50 | 3.41 | 3.17 | 2.32 |
| PEER1078 | | | | | | | | 5.37 | |
| PEER1116 | | 3.22 | 2.57 | | 2.73 | 3.88 | | 3.25 | 3.82 |
| PEER1144 | 9.16 | 10.41 | 10.46 | 9.07 | 12.45 | 10.37 | | | 10.65 |
| PEER1776 | 12.28 | 13.55 | 12.54 | 12.06 | 11.65 | 15.52 | 10.20 | 11.68 | 12.95 |
| PEER1794 | | 5.01 | 5.29 | | 6.43 | 4.60 | | 3.79 | 3.85 |
| PEER1795 | 14.74 | | | 14.62 | | | 14.22 | | 21.89 |
| TGMB1584 | | | 8.05 | | | | | | |
| TGMB1585 | | | | | | | | | |
| TGMB1591 | | | | | | | | 11.13 | |
| TGMB1594 | | | | | | | | | |



DOI: 10.1002/eqe

Cimellaro [37] for the broader Europe region. The selected records as well as the scaling factors did not change except for one record for 4-story and 8-story models. This additional case study certifies the stability of our analysis in terms of CMS-based record selection and scaling.

*3.3.2. Comparisons of results.* Nonlinear equivalent SDOF and MDOF RHA of model buildings are performed by using the optimum ground-motion records selected and scaled according to each methodology: Ay and Akkar [12], AA12, Baker [5], B11, and Kalkan and Chopra [20], KC11. Figure 3 summarizes the results of these analyses. The first column panels describe the elastic median and dispersion statistics computed from linear SDOF RHA. These panels also show the target elastic spectral ordinate (indicated by black dashed lines). Although the elastic response is not the actual focus of the case study, the first column panels serve for a complete picture about the performance of each method as the state-of-the-art hazard studies almost always define elastic target hazard for ground-motion scaling purposes. The second column panels on Figure 3 show the median inelastic spectral displacements, and the dispersion about the median computed from the nonlinear SDOF RHA of the idealized building models. (See Ay [14] for the idealized SDOF behavior of each building model). The third column panels of the same figure display the MRDR statistics computed from the MDOF nonlinear RHA. The solid squares on Figure 3 define the median response parameters, whereas the error bars show the ± one standard deviation about median response. The cross symbols in gray show the scatter in response about median. The Ay and Akkar [12] procedure can also estimate the median response and its standard deviation (Equations (5) and (6)) for

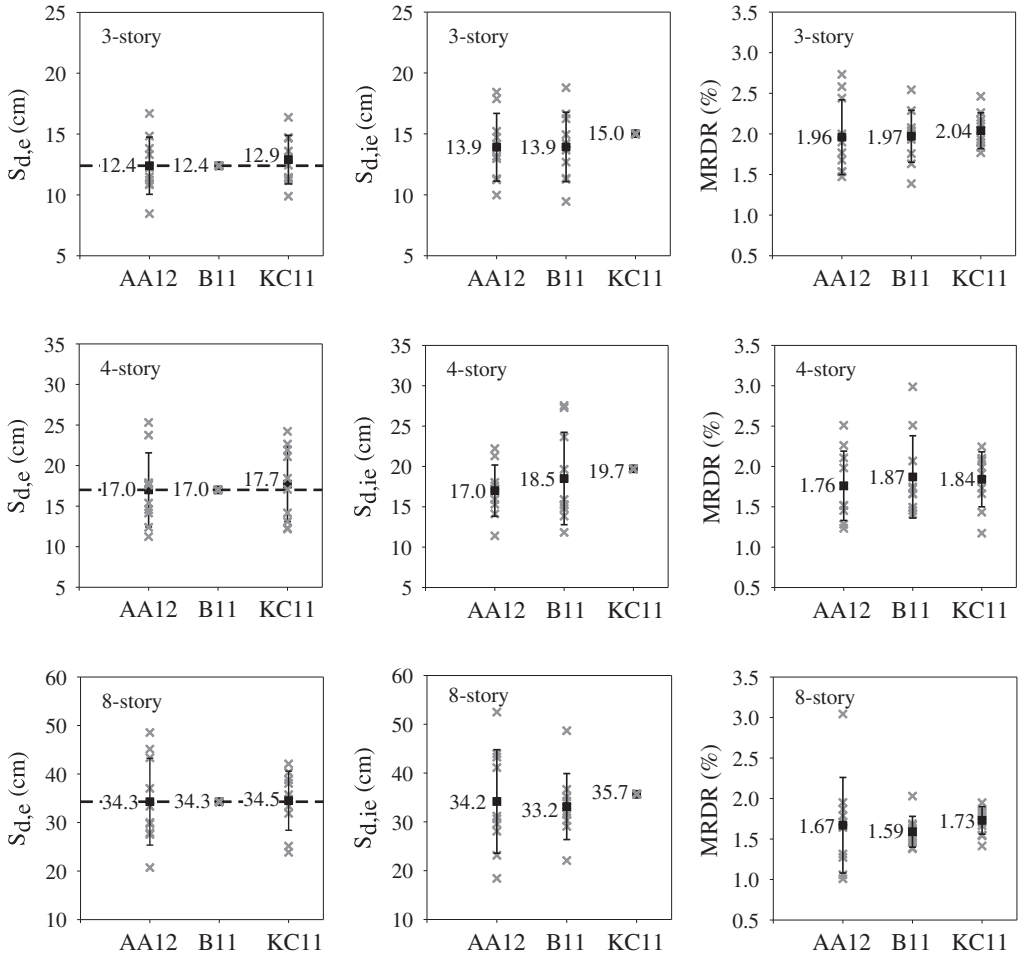


Figure 3. Comparisons of linear (first column), nonlinear (second column) SDOF responses, and MDOF RHA (third column) results obtained from alternative record selection and scaling procedures.



DOI: 10.1002/eqe

equivalent SDOF response of linear and nonlinear cases. However, these values are not given on the plots as the other two methods (B11 and KC11) do not have such a feature. The advantage of estimating the median and standard deviation of SDOF response by AA12 is discussed in the next section.

The nonlinear SDOF response results presented in the second column panels of Figure 3 indicate that all three selection and scaling procedures yield fairly similar results in terms of median nonlinear spectral response. Among these, Kalkan and Chopra [20] resulted in slightly larger median structural response. Note that AA12 and B11 scale the records such that the average elastic spectral ordinates of the modified records match exactly with the target elastic spectral ordinate (see first column panels of Figure 3). Kalkan and Chopra [20] iteratively scale the records to the inelastic target level that is estimated from an empirical $C_R$ expression. Thus, the average elastic spectral response of the records selected and scaled by KC11 does not necessarily match with the target elastic spectral ordinate (see first column panels of Figure 3). This observation brings forward the significance of accuracy in the empirical $C_R$ equation used for obtaining the inelastic target level. In this study, the empirical elastic-to-inelastic spectral conversion equation proposed by Chopra and Chintanapakdee [38], CC04, is used to obtain the target inelastic spectral displacements. Equation (7) shows the empirical $C_R$ expression proposed by Chopra and Chintanapakdee [38]. The parameters α, R, $T_n$, and $T_c$ refer to post-yield stiffness ratio, strength reduction factor, fundamental period of the idealized system, and corner period separating the acceleration and velocity-sensitive regions of the target spectrum, respectively. The coefficients a, b, c, and d are taken as 61, 2.4, 1.5, and 2.4, respectively, according to Chopra and Chintanapakdee [38]. On average, the empirical $C_R$ relationship by Chopra and Chintanapakdee [38] tends to overestimate the inelastic SDOF response up to 8% for buildings and 14% for bridges [39].

$$C_R = 1 + \left[ \left( \left( \frac{1}{R} \left( 1 + \frac{R-1}{\alpha} \right) \right) - 1 \right)^{-1} + \left( \frac{a}{R^b} + c \right) \left( \frac{T_n}{T_c} \right)^d \right]^{-1} \tag{7}$$

As one can infer from the nonlinear SDOF dispersion behavior, the resulting scatter in AA12 is slightly lesser than that of B11 for shorter vibration periods ($T_1 < 0.9$ s). The increase in period (i.e., $T_1 \geq 0.9$ s) decreases the efficiency of $\varepsilon\sigma_{ISd}$, which results in relatively larger scatter in the records modified by AA12 when compared to B11. The dispersion is zero in KC11 for nonlinear SDOF response because the scaling of each accelerogram is peformed to have a one-to-one match with the inelastic target response displacement. The MDOF RHA results presented on the third column panels of Figure 3 follow similar trends to those of nonlinear SDOF response statistics. This observation will be used in the following section while deriving the likelihood of damage states by AA12. The outcomes of MDOF RHA indicate that the compared selection and scaling methods result in comparable median MRDR values. Among the compared methodologies, the minimum dispersion is achieved by KC11 for all three buildings. Thus, the dispersion about median structural response statistics presented in Figure 3 may favor KC11 with respect to the other two procedures. However, the dependency of KC11 on the empirical elastic-to-inelastic spectral conversion factors is worth to be considered for a full evaluation of this method. The accuracy in empirical $C_R$ can introduce an additional uncertainty to the structural response statistics. To this end, KC11 is reevaluated by using two alternative elastic-to-inelastic spectral conversion equations proposed by Ruiz-García and Miranda [40] and Krawinkler and Nassar [41]. These alternative expressions are designated as RM07 [40] and KN92 [41] in the text. The latter elastic-to-inelastic spectral conversion factor is one of the well-known $R_\mu$-$\mu$-$T$ relationships. It requires displacement ductility ratio ($\mu$) for computing the expected inelastic spectral displacement for a given $R$ [42]. The displacement ductility ratio of each building model can be achieved from their idealized capacity curves. Table V lists the target inelastic spectral displacements ($\overline{S}_{dit\,arget}$) of each model computed from the corresponding elastic target spectral displacements ($\overline{S}_{dt\,arget}$) for the three empirical elastic-to-inelastic spectral conversion equations.



DOI: 10.1002/eqe

Table V. Target elastic spectral displacements ($\overline{S}_{dt\,\mathrm{arget}}$) and corresponding inelastic target spectral displacements ($\overline{S}_{dit\,\mathrm{arget}}$) of alternative empirical elastic-to-inelastic spectral conversion equations.

| | 3-story | 4-story | 8-story |
|---|---|---|---|
| $\overline{S}_{dt\,\mathrm{arget}}(T_1)$ | 12.4 cm | 17.0 cm | 34.3 cm |
| $\overline{S}_{dit\,\mathrm{arget}}(T_1)$ according to [38] | 15.0 cm | 19.7 cm | 35.7 cm |
| $\overline{S}_{dit\,\mathrm{arget}}(T_1)$ according to [40] | 15.5 cm | 20.6 cm | 36.8 cm |
| $\overline{S}_{dit\,\mathrm{arget}}(T_1)$ according to [41] | 10.5 cm | 16.9 cm | 31.5 cm |

The $\overline{S}_{dit\,\mathrm{arget}}$ estimated by KN92 differs significantly from those of the other two $C_R$ expressions particularly for the 3-story model.

Figure 4 presents the median MRDR values and corresponding dispersions computed from the nonlinear RHA of 3-story building by using the selected and scaled accelerograms of KC11 with three empirical elastic-to-inelastic spectral conversion equations: CC04, RM07, and KN92. The scatter plots on Figure 4 depict that the use of different elastic-to-inelastic spectral conversion expressions may result in a variation in the median MRDR and corresponding dispersion statistics. MRDR statistics obtained from the use of CC04 and RM07 empirical spectral conversion factors are similar to each other, but this is not the case when KN92 is employed to compute the target inelastic spectral displacement. The median MRDR obtained by the use of KN92 is approximately 40% less than those of CC04 and RM07. The shortcoming of such a difference can be reflected on damage assessment studies as likelihoods of damage states can vary depending on the target inelastic deformation estimated by the chosen $C_R$ expression. Neither AA12 nor B11 would run into this type of problem as their record selection and scaling directly relies on elastic spectral ordinates.

## 4. PROPOSED SELECTION AND SCALING METHOD AS A TOOL FOR PROBABILISTIC DAMAGE ASSESSMENT AND LOSS MODELS

Given a target intensity measure the probability-based damage assessment of structures requires the determination of exceedance probability of a structural response measure at a certain limit state. Exceedance probabilities for different levels of chosen ground-motion intensity parameter result in fragility functions that can be used in probabilistic loss models. Equation (8) defines the fragility

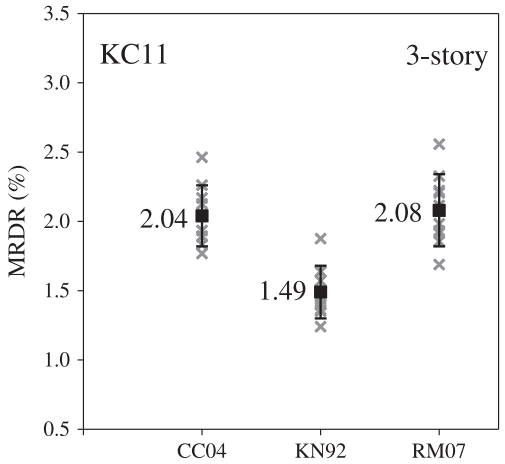


Figure 4. Nonlinear RHA results of 3-story frame obtained from KC11 method by employing alternative empirical elastic-to-inelastic spectral displacement ratios. CC04, KN92, and RM07 refer to Chopra and Chintanapakdee [38], Krawinkler and Nassar [41], and Ruiz-García and Miranda [40], respectively.



DOI: 10.1002/eqe

function for the exceedance probability of MRDR (structural response measure) under a limit state conditioned on spectral displacement (ground-motion intensity parameter).

$$\text{Fragility} = \text{P}\left(\text{MRDR} \geq \text{Limit State} | S_{\text{dt arget}}\right) \tag{8}$$

The selection and scaling methodology proposed by Ay and Akkar [12] can estimate the distribution of nonlinear structural response parameters of interest through the expressions given in Equations (5) and (6). This section investigates the reliability of these estimations for probability-based rapid seismic performance assessment. The final part discusses the use of proposed record selection and scaling procedure in the derivation of site-specific (or region-specific) fragility curves.

The already presented case study in Section 3 is employed to compute the damage probabilities that are obtained from the probability distribution parameters estimated from Equations (5) and (6). These probability distributions are compared with those obtained from the results of nonlinear RHA. The record selection and scaling methods by Baker [5] and Kalkan and Chopra [20] are also involved in the comparisons to have a broader picture about the performance of the proposed procedure.

### *4.1. Limit states*

In order to evaluate the performance of the Ay and Akkar [12] procedure as a tool in damage probability assessment, three limit state definitions for RC MRF models are used. The limit states are defined as immediate occupancy, life safety, and collapse prevention. It is assumed that structures having no or slight damage perform at immediate occupancy limit state, whereas structures at life safety and collapse prevention limit states are assumed to sustain significant and severe damages, respectively. The structures are considered as collapsed beyond collapse prevention limit state. In essence, four damage states can be defined as no or slight damage (DS1), significant damage (DS2), severe damage (DS3), and collapse (DS4).

The limit state values of RC MRF structures in Turkey are investigated previously by several publications. These studies reveal that the limit state determination for RC MRF buildings involves significant uncertainty [43]. Following the recommendations of Ay and Erberik [43], three criteria are employed to specify the structural performance levels. These are the accumulation of damage in structural members, the softening index, which is introduced by Dispasquale and Çakmak [44] and the ductility level [45] of the structure. The performance limits are specified in accordance with these criteria, and then they are converted to MRDR values for each limit state. Although identification of limit states may vary from one method to the other, the specific features of these calculations cannot be covered within this paper due to space limitations. It is noted that the suggested methodology in this section is independent of quantitative variations in each limit states provided that they are physically meaningful in terms of engineering perspective. The reader is referred to Ay and Erberik [43] about the details of the criteria employed in the identification of limit states. Table VI lists the MRDR values (in percent) associated with the immediate occupancy, life safety, and collapse prevention performance levels for the three frame models. The suggested MRDR values for different limit states show similarity with those suggested by Booth *et al*. [46] as well as Ay and Erberik [43].

Table VI. Maximum roof drift ratios that describe immediate occupancy, life safety, and collapse prevention structural limit states.

| | Maximum roof drift ratio (%) | | |
|---|---|---|---|
| Model frame | Immediate occupancy* | Life safety* | Collapse prevention* |
| 3-story | 0.62 **(4.17)** | 1.47 **(9.89)** | 2.87 **(19.30)** |
| 4-story | 0.55 **(4.90)** | 1.32 **(11.77)** | 2.82 **(25.14)** |
| 8-story | 0.45 **(7.95)** | 0.96 **(16.96)** | 2.02 **(35.70)** |

*Bold numbers in parenthesis are the corresponding inelastic spectral displacements (cm) as explained in Section 4.2.



DOI: 10.1002/eqe

### 4.2. Probabilistic damage assessment results

Response history analysis results of frame models with the records selected and scaled according to the compared methods are presented in the previous section. One of the major advantages of the Ay and Akkar [12] method is its ability to estimate the distribution of nonlinear structural response by making analogy with the distribution of scaled ground-motion intensity parameter. Thus, there is no need to perform detailed nonlinear MDOF RHA for establishing the likely damage state of a given building. Assuming the distribution of structural response parameter (MRDR in this study) is log-normal, Equations (5) and (6) estimate its median and logarithmic standard deviation for the given target spectral displacement. This information can be employed to calculate the damage state probabilities through Equations (9)–(12). The computed probabilities from these equations are used to evaluate the performance of the Ay and Akkar [12] procedure as a tool for probabilistic damage assessment.

$$\mathrm{DS1} = \mathrm{P}\left(\mathrm{MRDR} \leq \mathrm{IO} | \mathrm{S}_{\mathrm{dt\,arget}}\right) \tag{9}$$

$$\mathrm{DS2} = \mathrm{P}\left(\mathrm{IO} \leq \mathrm{MRDR} \leq \mathrm{LS} | S_{\mathrm{dt\,arget}}\right) \tag{10}$$

$$\mathrm{DS3} = \mathrm{P}\left(\mathrm{LS} \leq \mathrm{MRDR} \leq \mathrm{CP} | S_{\mathrm{dt\,arget}}\right) \tag{11}$$

$$\mathrm{DS4} = \mathrm{P}\left(\mathrm{MRDR} > \mathrm{CP} | S_{\mathrm{dt\,arget}}\right) \tag{12}$$

As noted previously, Equations (5) and (6) estimate the median and logarithmic standard deviation of scaled inelastic spectral displacements to obtain their probability distributions for a given elastic target intensity level. Thus, an intermediate step is required to adjust the SDOF information (inelastic spectral displacement distribution) to MDOF response (MRDR distribution). The ADRS [31] constitutes the backbone of this intermediate step. The limit states defined in Table VI are modified for SDOF response quantities through ADRS, and they are used together with the computed median and logarithmic standard deviation values (i.e., probability distributions per Equations (5) and (6)) to estimate the damage state probabilities. Figure 5 compares the damage state probabilities estimated from the proposed methodology ($\mathrm{AA12_{EST}}$) and those computed from the execution of MDOF RHA of accelerograms selected and scaled by each procedure (AA12, B11 and KC11).

The results presented in Figure 5 show that the maximum difference between damage state probabilities obtained from the estimations of the Ay and Akkar [12] procedure, and the observed data is less than 10% for almost all cases. The difference in damage probabilities reaches to 13% only for the 8-story model. Considering the computation time and uncertainties involved in the nonlinear RHA of structures, these differences can be accepted as tolerable. Note that, the estimated damage state probabilities ($\mathrm{AA12_{EST}}$) are calculated from the approximate distributions that are provided to the analyst through simple calculations (Equations (5) and (6)) and adjustments (i.e., use of ADRS to convert MDOF response to SDOF response) under a given elastic spectral target value, fundamental period, and strength reduction factor. The damage state probabilities obtained from the selected and scaled records of AA12, B11, and KC11 through nonlinear MDOF RHA would require a significant computational effort, which certifies once again the practicality of the estimated damage state probabilities through Equations (5) and (6). Thus, the computational efficiency of the approximations brought by Ay and Akkar [12] can be very useful for rapid assessment of probabilistic damage distributions of large building stocks immediately after an earthquake.

### 4.3. Generation of site-specific and region-specific fragility curves

As given in Equation (8), fragility functions describe the exceedance probabilities for a set of damage states conditioned on different levels of a selected ground-motion intensity parameter. They can be



DOI: 10.1002/eqe

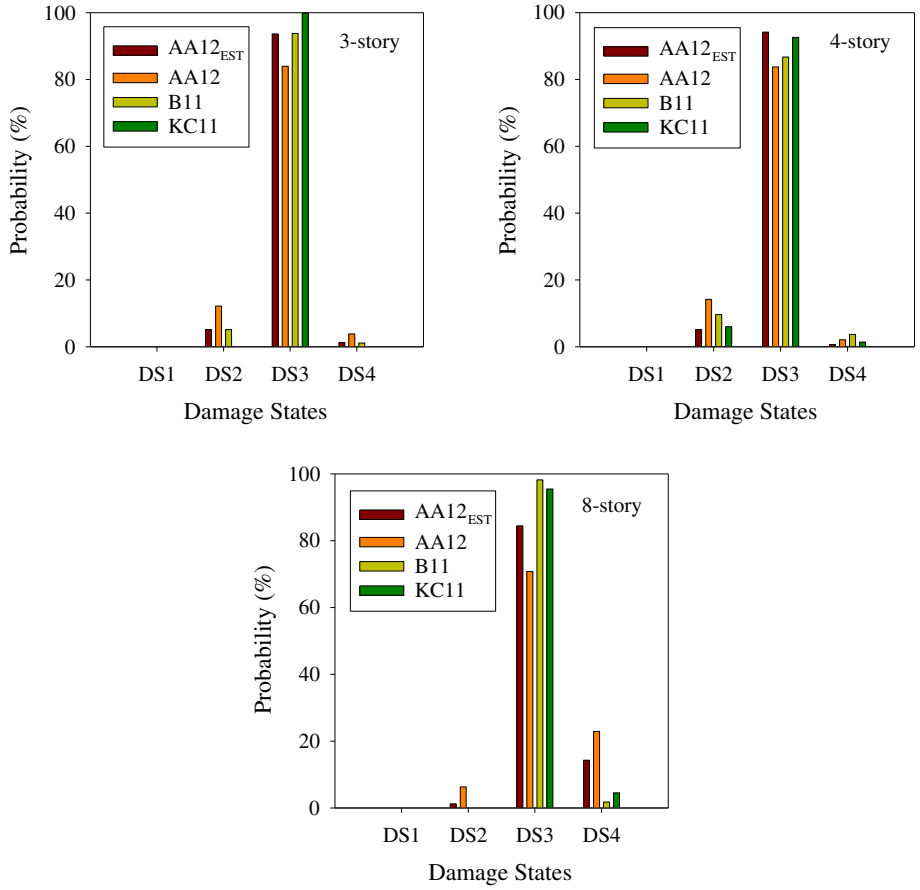


Figure 5. Damage state probabilities obtained from different approaches. $AA12_{EST}$ is the approximate damage state probability computed from Equations (5) and (6). AA12, B11, and KC11 refer to the damage probabilities obtained from the nonlinear MDOF RHA of the selected and scaled accelerograms by using the Ay and Akkar [12], Baker [5], and Kalkan and Chopra [20] methods, respectively.

converted into vulnerability functions that, in turn, are used in loss assessment. Within this context, loss estimations specific to a region or site would be more meaningful if fragilities provide consistent and accurate information between the exceedance probabilities of selected ground-motion intensity parameter and damage states. This point emphasizes the significance of selected ground-motion records while establishing the fragility functions.

Currently, the selection of accelerograms for generating fragilities does not follow a formal procedure. Most studies in this field prefer using real accelerograms and scale them in an arbitrary manner to cover the range of ground-motion levels that might occur in the region of interest (e.g., [47]). Alternatively, some researchers disregard scaling and assemble a set of accelerograms with increasing amplitudes of the selected ground-motion intensity parameter (e.g., [48]). As discussed briefly in the introductory section, the latter approach may not always yield a sufficient number of accelerograms that satisfy all the seismological constraints put forward by a region-specific or site-specific study. The former approach should be applied carefully in order not to use excessive scaling factors as they may distort the genuine characteristics of accelerograms leading to misrepresentation of actual building behavior [49]. Moreover, none of these procedures quantitatively establishes a relationship between the exceedance probabilities of ground-motion intensity parameter and damage states.

The success of estimating the probabilities of damage states by the proposed procedure inspired the authors to use it as a tool for consistent site-specific or region-specific fragility function generation. The entire methodology that is tailored to achieve this objective is shown in Figure 6. Given a site-specific PSHA study, one can determine the hazard curve that would reveal the expected annual exceedance



DOI: 10.1002/eqe

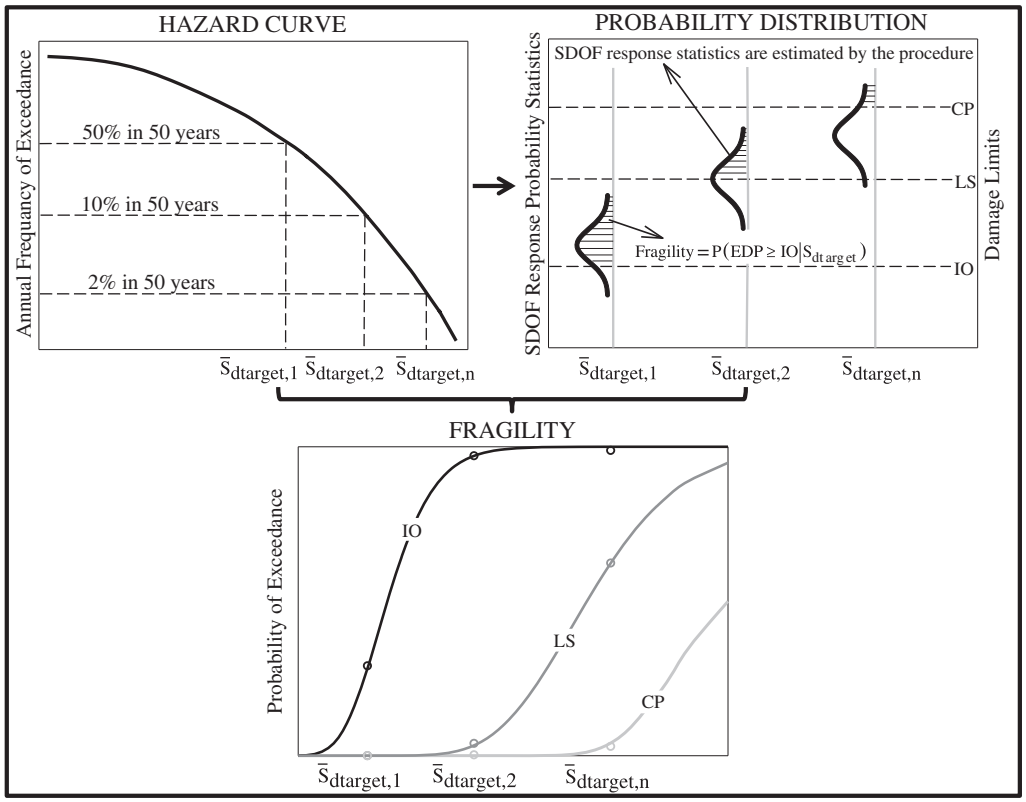


Figure 6. Schematic representation of site-specific or region-specific fragility functions by making use of the proposed record selection and scaling procedure.

rates of the selected ground-motion intensity parameter (e.g., spectral displacement, $S_d$) of different amplitudes (upper left panel on Figure 6). Each one of these amplitudes can be interpreted as a target hazard level with a known exceedance probability for a certain exposure time (e.g., 2% exceedance probability for an economic lifespan of 50 years; upper left panel on Figure 6). The proposed procedure can then be utilized to select and scale the optimum set of ground-motion records that essentially match with each target hazard level. As the procedure can make a reasonable estimation about the probability distribution of scaled spectral ordinates about each target hazard level, one can easily convert this information into the likely damage states for predetermined damage limits (upper right panel on Figure 6). This step is followed by the construction of probability curves for different damage states as their exceedance probabilities for each target hazard level ($\overline{S}_{dt\,arget}$) are already calculated (lower middle panel on Figure 6). The presented methodology establishes a direct relationship between the exceedance probabilities of ground-motion intensity parameter and damage states, which can be considered as an important advantage for deriving realistic site-specific fragility functions of important structures. It can also be used for more efficient probabilistic risk assessment of large building stocks in a particular region.

Figure 7 presents a case study on the implementation of above methodology for computing the site-specific fragilities of the building models used in this paper. The probabilistic seismic hazard study is the same one discussed in Section 3.2. Therefore, the fragility functions can be used to assess the probabilistic seismic risk of code-complying MRF building stock located on soft soil sites in the city of Erzurum. The spectral displacement hazard curves of $T_1 = 0.5$ s (3-story), $T_1 = 0.61$ s (4-story), and $T_1 = 1.12$ s (8-story) are used to compute spectral ordinates representing a set of return periods of frequent to rare events (i.e., $T_R = 72$, 225, 475, 975, 1225, 1642, and 2475 years). For each spectral ordinate, the optimum ground-motion bin is selected and scaled from the candidate accelerograms given in Table III. The probability distributions of scaled records are computed from Equations (5) and (6) that are used in estimating the exceedance probability of limit states (i.e., immediate



DOI: 10.1002/eqe

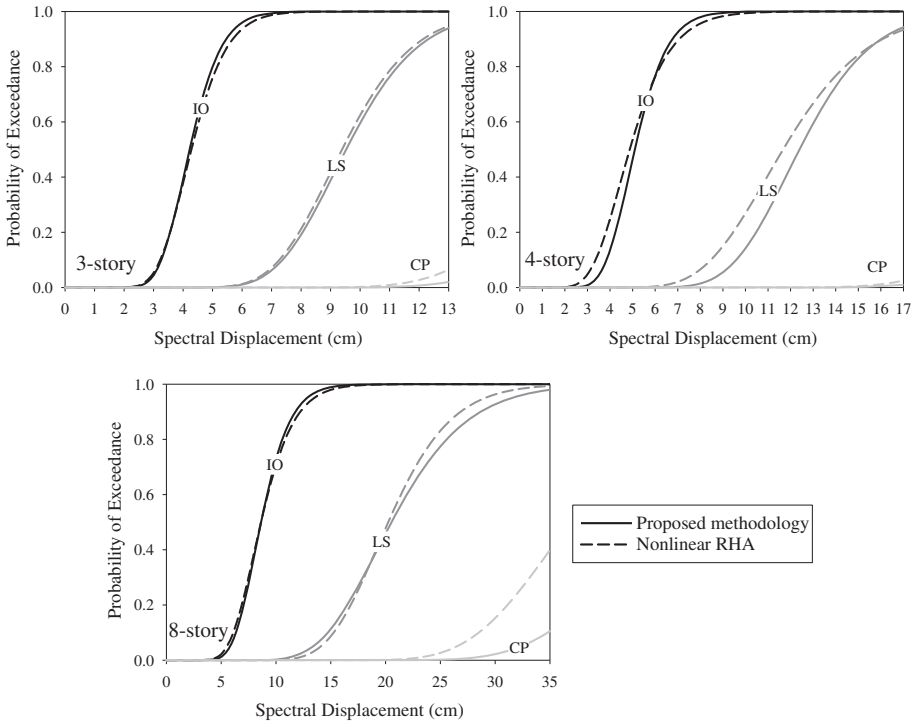


Figure 7. Computation of site-specific fragility functions for immediate occupancy (IO), life safety (LS), and collapse prevention (CP) for low-rise and mid-rise MRF buildings that are located on soft site class in the city of Erzurum. Solid lines represent the fragilities obtained from the proposed methodology, and dashed lines are the fragilities computed from nonlinear RHA.

occupancy, life safety, and collapse prevention). The estimated damage probabilities are then combined with the corresponding target spectral displacement ordinates ($\overline{S}_{dt\,arget}$), and a log-normal probability curve is fitted (solid lines on Figure 7) to these points to establish the site-specific fragilities for each frame. The dashed lines on these panels represent the fragilities obtained from the nonlinear RHA by using the scaled accelerograms for each target spectral ordinate. The computational time of establishing fragility functions from RHA is 70 times slower than the approach proposed in this section. When fragility functions of proposed approach is compared with those of nonlinear RHA, the similarity in their behavior is significant suggesting the success of proposed record selection and scaling approach in deriving coherent site-specific or region-specific fragility functions. This observation is highlighted in Table VII that gives the median (θ) and log-normal standard deviation (β) values of the fragility functions derived from nonlinear RHA as well as Equations (5) and (6). The fragility function parameters computed from nonlinear RHA are designated as 'observed' in

Table VII. Log-normal distribution parameters of fragility functions that are obtained from nonlinear RHA (Observed) and proposed method (Estimated).

| | | Immediate occupancy | | Life safety | | Collapse prevention | |
|---|---|---|---|---|---|---|---|
| Model frame | Fragility curve parameters | Estimated | Observed | Estimated | Observed | Estimated | Observed |
| 3-story | θ | 1.44 | 1.46 | 2.25 | 2.24 | 2.98 | 2.87 |
| | β | 0.20 | 0.22 | 0.20 | 0.20 | 0.20 | 0.20 |
| 4-story | θ | 1.63 | 1.58 | 2.52 | 2.46 | 3.30 | 3.23 |
| | β | 0.22 | 0.29 | 0.20 | 0.25 | 0.20 | 0.20 |
| 8-story | θ | 2.16 | 2.16 | 3.02 | 3.01 | 3.81 | 3.61 |
| | β | 0.24 | 0.27 | 0.26 | 0.22 | 0.20 | 0.20 |



DOI: 10.1002/eqe

Table VII, whereas the 'estimated' columns give the parameters derived by using structural response estimations of Equations (5) and (6), respectively. The similarity in fragility trends between the proposed methodology and those of nonlinear RHA perish for the collapse prevention limit state of the 8-story building. The computed fragility functions indicate that the likelihood of collapse in code-confirming low-rise and mid-rise MRF buildings in the city of Erzurum is significantly low even for spectral demands of $T_R = 2475$ years.

## 5. SUMMARY AND CONCLUSIONS

The record selection and scaling procedure proposed by Ay and Akkar [12] are evaluated for its use in probabilistic risk assessment studies. A computer program with a user-friendly graphical interface of the procedure is available at http://www.metu.edu.tr/~ozer/documents/sources/ReSaS.rar. The Ay and Akkar procedure scales ground motions for a given target elastic spectral ordinate without suppressing the aleatory variability. It estimates the distribution of scaled accelerograms about target hazard level to describe inherent ground-motion uncertainty. The distribution of scaled ground motions is estimated not only for elastic structural behavior but also for structures responding beyond their elastic limits. Whether the structural response is linear or nonlinear, the Ay and Akkar [12] procedure tailors the ground-motion scaling by considering the elastic target hazard level. In other words, the average of scaled ground motions will always match the elastic target spectral ordinate, but the estimated ground-motion response is described according to the actual structural behavior. This approach is advantageous as the state-of-art seismic hazard assessment, almost exclusively, describes the ground-motion hazard by elastic spectral ordinates.

The Ay and Akkar [12] procedure is evaluated by using low-rise and mid-rise RC MRF buildings that comply with the Turkish design codes. The performance verifications are performed in a comparative manner by considering two alternative record selection and scaling procedures proposed by Baker [5] and Kalkan and Chopra [20]. The scaling procedure by Baker [5] relies on CMS.[‡] Although the theoretical backgrounds of the Ay and Akkar [12] and Baker [5] record selection and scaling procedures are different, both methods make use of target elastic spectral ordinates in record scaling. Kalkan and Chopra [20] first estimate the target inelastic spectral ordinates from empirical elastic-to-inelastic conversion factors and then implement an iterative procedure to scale the records to the estimated inelastic target level. The results of nonlinear equivalent SDOF and MDOF RHA indicate a fairly similar performance of the Ay and Akkar [12] and Baker [5] procedures, although there are spectral period intervals where the scatter of scaled ground motions resulting from one of these methods is slightly lesser than the other one. The records scaled by Kalkan and Chopra [20] show minimum dispersion about nonlinear target spectral displacement with respect to the other two methods. However, this method is sensitive to the selected empirical elastic-to-inelastic spectral conversion relationship, which can change the level of target inelastic spectral displacement. This may, essentially, affect the damage assessment of a building as damage states depend on the target inelastic spectral level.

The observed similarity between the probability distributions of scaled ground-motion spectral ordinates and global structural demand parameters (e.g., MRDR) is utilized by the Ay and Akkar [12] procedure to estimate the nonlinear response distribution of structural models subjected to scaled accelerograms. The comparative results suggest that the probabilistic damage states identified from the approximate probability distributions provided by Ay and Akkar [12] are successful. Thus, this scaling procedure can be used as an auxiliary tool for probability-based seismic performance assessment. Conventional record selection and scaling procedures require nonlinear RHA for accomplishing the likelihoods of damage states for a given structural system. This fact makes the Ay and Akkar [12] procedure even more useful for rapid probabilistic damage assessment of large building stocks.

[‡]Note that Lin *et al*. [8] recently improved CMS for multiple seismic sources by using a set of GMPEs to account for the exact variability in target spectrum. The new spectrum by Lin et al. [8] is designated as conditional spectrum. However, CMS is still valid for the purposes of this study as it can approximate the exact conditional mean from a single GMPE when sites are dominated by a single seismic source, which is the case in our site-specific PSHA.



DOI: 10.1002/eqe

Given a target hazard level for a certain annual exceedance rate, the successful estimation of probability damage states led the use of Ay and Akkar [12] method for developing region-specific (or site-specific) fragility functions. This method can be implemented for selecting and scaling the optimum sets of records that essentially match with the discrete hazard levels obtained from a site-specific or region-specific PSHA study. Computing the probability curves for a set of predetermined damage states specific to a particular structural system or a building stock will essentially yield the subject fragility functions. The case study discussed in the text advocates the success of Ay and Akkar [12] record selection and scaling procedure for the derivation of rapid and accurate fragility functions that would result in useful information for loss estimation studies specific to a region or a site.

## ACKNOWLEDGEMENTS

The authors thank two anonymous reviewers for their constructive critiques and suggestions, which increase the technical quality of the paper.

## REFERENCES

1. Zareian F, Krawinkler H. Assessment of probability of collapse and design for collapse safety. *Earthquake Engineering and Structural Dynamics* 2007; **36**:1901–1914.
2. Cimellaro GP, Reinhorn AM, D'Ambrisi A, De Stefano M. Fragility analysis and seismic record selection. *Journal of Structural Engineering, ASCE* 2011; **137**(3):379–390.
3. Shome N, Cornell CA, Bazzurro P, Carballo JE. Earthquakes, records, and nonlinear responses. *Earthquake Spectra* 1998; **14**(3):469–500.
4. Naeim F, Alimoradi A, Pezeshk S. Selection and scaling of ground motion time histories for structural design using genetic algorithms. *Earthquake Spectra* 2004; **20**(2):413–426.
5. Baker JW. Conditional mean spectrum: tool for ground-motion selection. *Journal of Structural Engineering, ASCE* 2011; **137**(3):322–331. DOI: 10.1061/(ASCE)ST.1943-541X.0000215.
6. Jayaram N, Lin T, Baker JW. A computationally efficient ground-motion selection algorithm for matching a target response spectrum mean and variance. *Earthquake Spectra* 2011; **27**:797–815.
7. Lin T, Haselton CB, Baker JW. Conditional-spectrum-based ground motion selection. Part II: intensity-based assessments and evaluation of alternative target spectra. *Earthquake Engineering and Structural Dynamics* 2013. DOI: 10.1002/eqe.2303.
8. Lin T, Harmsen SC, Baker JW, Luco N. Conditional spectrum computation incorporating multiple causal earthquakes and ground-motion prediction models. *Bulletin of the Seismological Society of America* 2013; **103**(2A):1103–1116.
9. Kottke A, Rathje EM. A semi-automated procedure for selecting and scaling recorded earthquake motions for dynamic analysis. *Earthquake Spectra* 2008; **24**(4):911–932.
10. Buratti N, Stafford PJ, Bommer JJ. Earthquake accelerogram selection and scaling procedures for estimating the distribution of drift response. *Journal of Structural Engineering, ASCE* 2011; **137**(3):345–357.
11. Huang Y, Whittaker AS, Luco N, Hamburger RO. Scaling earthquake ground motions for performance-based assessment of buildings. *Journal of Structural Engineering, ASCE* 2011; **137**(3); 311–321.
12. Ay BÖ, Akkar S. A procedure on ground motion selection and scaling for nonlinear response of simple structural systems. *Earthquake Engineering and Structural Dynamics* 2012; **41**:1693–1707.
13. Aslani H, Cabrera C, Rahnama M. Analysis of the sources of uncertainty for portfolio-level earthquake loss estimation. *Earthquake Engineering and Structural Dynamics* 2012; **41**:1549–1568.
14. Ay BÖ. A proposed ground motion selection and scaling procedure for structural systems. *Ph.D. Thesis*, Middle East Technical University, Ankara, Turkey, 2012.
15. Tothong P, Cornell AC. An empirical ground-motion attenuation relation for inelastic spectral displacement. *Bulletin of the Seismological Society of America* 2006; **96**(6):2146–2164.
16. Bozorgnia Y, Hachem MM, Campbell KW. Ground motion prediction equation ("attenuation relationship") for inelastic response spectra. *Earthquake Spectra* 2010; **26**(1):1–23.
17. Rupakhety R, Sigbjörnsson R. Ground-motion prediction equations (GMPEs) for inelastic response and structural behaviour factors. *Bulletin of Earthquake Engineering* 2009; **7**:637–659.
18. Rupakhety R, Sigbjörnsson R. Ground-motion prediction equations (GMPEs) for inelastic displacement and ductility demands of constant-strength SDOF systems. *Bulletin of Earthquake Engineering* 2009; **7**:661–679.
19. Goda K, Atkinson GM. Seismic demand estimation of inelastic SDOF systems for earthquakes in Japan. *Bulletin of the Seismological Society of America* 2009; **99**(6):3284–3299.
20. Kalkan E, Chopra AK. Modal-pushover-based ground motion scaling procedure. *Journal of Structural Engineering, ASCE* 2011; **137**(3):298–310.
21. Ministry of Public Works and Settlement. Specification for buildings to be built in seismic zones TEC-07, Ankara, Turkey, 2007.
22. Turkish Standards Institute. TS 500-2000, Requirements for design and construction of reinforced concrete structures, Ankara, Turkey, 2000.

23. Turkish Standards Institute. TS 498, Design loads for buildings, Ankara, Turkey, 1997.
24. Probina Orion - Software for analysis, design and detailing of building systems, version V16-sp6, Prota Software Inc., Ankara, Turkey, 2012.
25. SeismoStruct - A Computer program for static and dynamic nonlinear analysis of framed structures, Seismosoft, Pavia, Italy, 2012.
26. Hilber HM, Hughes TJR, Taylor RL. Improved numerical dissipation for time integration algorithms in structural dynamics. *Earthquake Engineering and Structural Dynamics* 1977; **5** (3):283–292.
27. Spacone E, Ciampi V, Filippou FC. Mixed formulation of nonlinear beam finite element. *Computers and Structures* 1996; **58**(1):71–83.
28. Mander JB, Priestley MJN, Park R. Theoretical stress-strain model for confined concrete. *Journal of Structural Engineering* 1988; **114**(8):1804–1826.
29. Chopra AK, Goel RK. A modal pushover analysis procedure for estimating seismic demands for buildings, *Earthquake Engineering and Structural Dynamics* 2002; **31**(3):561–582.
30. Applied Technology Council (ATC). Seismic evaluation and retrofit of concrete buildings, ATC-40, report No: SSC 96-01, Redwood City, CA, 1996.
31. Mahaney JA, Paret TF, Kehoe BE, Freeman SA. The capacity spectrum method for evaluating structural response during the Lorna Prieta Earthquake. *1993 National Earthquake Conference*, Memphis, USA, 1993.
32. Akkar S, Bommer JJ. Empirical equations for the prediction of PGA, PGV, and spectral accelerations in Europe, the Mediterranean Region, and the Middle East. *Seismological Research Letters* 2010; **81**(2):195–206.
33. Joyner WB, Boore DM. Peak horizontal acceleration and velocity from strong-motion records including records from the 1979 Imperial Valley, California, Earthquake. *Bulletin of the Seismological Society of America* 1981; **71**(6):2011–2038.
34. Building Seismic Safety Council (BSSC). *NEHRP Recommended Provisions for Seismic Regulations for New Buildings and Other Structures FEMA P-750*. Federal Emergency Management Agency: Washington, DC, 2009.
35. Baker JW, Cornell CA. Correlation of response spectral values for multi-component ground motions. *Bulletin of the Seismological Society of America* 2006; **96**(1):215–227.
36. Ruiz-García J, Miranda E. Inelastic displacement ratios for evaluation of existing structures. *Earthquake Engineering and Structural Dynamics* 2003; **32**(8):1237–1258.
37. Cimellaro GP. Correlation in spectral accelerations for earthquakes in Europe. *Earthquake Engineering and Structural Dynamics* 2013; **42**(4):623–633.
38. Chopra AK, Chinatanapakdee C. Inelastic deformation ratios for design and evaluation of structures: single-degree-of-freedom bilinear systems. *Journal of Structural Engineering, ASCE* 2004; **130**(9):1309–1319.
39. Kalkan E, Chopra AK. *Practical Guidelines to Select and Scale Earthquake Records for Nonlinear Response History Analysis of Structures, USGS Open-File Report 2010-1068*. U.S. Geological Survey: Reston, Virginia, 2010; 126 pp.
40. Ruiz-García J, Miranda E. Probabilistic estimation of maximum inelastic displacement demands for performance-based design. *Earthquake Engineering and Structural Dynamics* 2007; **36**:1235–1254.
41. Krawinkler H, Nassar AA. Seismic based design on ductility demand and cumulative damage demands and capacities. In *Non-linear Seismic Analysis and Design of Reinforced Concrete Buildings*, Fajfar P, Krawinkler H (eds). Elsevier Science: New York, 1992.
42. Miranda E. Estimation of inelastic deformation demands of SDOF systems. *Journal of Structural Engineering, ASCE* 2001; **127**(9):1005–1012.
43. Ay BÖ, Erberik MA. Vulnerability of Turkish low-rise and mid-rise reinforced concrete frame structures. *Journal of Earthquake Engineering* 2008; **12**(S2):2–11.
44. DiPasquale E. Çakmak AS. Detection and assessment of seismic structural damage. *Technical Report NCEER–87–0015*, State University of New York, Buffalo, NY, 1987.
45. Calvi GM. A displacement–based approach for vulnerability evaluation of classes of buildings. *Journal of Earthquake Engineering* 1999; **3**(3):411–438.
46. Booth E, Spence R, Bird J. Building vulnerability assessment using pushover methods – a Turkish case study. *Proceedings of an International Workshop on Performance–Based Seismic Design Concepts and Implementation*, Bled, Slovenia, 2004; 397–408.
47. Dumova-Jovanoska E. Fragility curves for reinforced concrete structures in Skopje (Macedonia) Region. *Soil Dynamics and Earthquake Engineering* 2000; **19**:455–466.
48. Akkar S, Sucuoglu H, Yakut A. Displacement-based fragility functions for low- and mid-rise ordinary concrete buildings. *Earthquake Spectra* 2005; **21**(4):901–927.
49. Ay BÖ, Akkar S. Selecting and scaling of real accelerograms to reduce the scatter in dynamic response. *Proceedings of the 9th U.S. National and 10th Canadian Conference on Earthquake Engineering*, Toronto, Canada, 2010; Paper No: 920, 10 pp.



DOI: 10.1002/eqe